coatings

MDPI

Article

Durable Superhydrophobic Coating for Efficient Microplastic Removal

Oriol Rius-Ayra *, Alisiya Biserova-Tahchieva and Nuria Llorca-Isern

CMQF Departament de Ciència dels Materials i Química Física, Facultat de Química, Universitat de Barcelona, Marti i Franquès 1, 08028 Barcelona, Spain; abiserova.tahchieva@ub.edu (A.B.-T.); nullorca@ub.edu (N.L.-I.)
* Correspondence: oriolriusayra@ub.edu

Abstract: The pollution caused by microplastics around the world is an increasingly significant issue that has to be tackled with different methods and technologies. Here, we report a straightforward and rapid process combining electrodeposition and electrophoresis to produce a durable superhydrophobic coating on an aluminum substrate (UNS A91070) that has a static contact angle (153°), sliding angle (1°), and contact angle hysteresis (1°). Field emission scanning electron microscopy and high-resolution transmission electron microscopy showed the presence of a hierarchical structure with nanolayers that were 70 nm thick. The chemical composition was also analyzed using attenuated total reflectance-Fourier transform infrared spectroscopy and high-resolution X-ray photoelectron spectroscopy, which revealed that the hierarchical structure was composed of zinc laurate ($Zn(C_{11}H_{20}COO)_2$) that decreased the surface free energy of the system. Moreover, the coating showed high durability against abrasion caused by the P1200 SiC paper due to the presence of TiO_2 particles in the upper layers as well as the homogeneous chemical composition of the hierarchical structure. Finally, taking advantage of the superoleophilic properties of superhydrophobic surfaces, the ability of the coating to remove high-density polyethylene microplastics from water was studied.

Keywords: superhydrophobic; superoleophilic durability; oil/water separation; microplastics

Citation: Rius-Ayra, O.; Biserova-Tahchieva, A.; Llorca-Isern, N. Durable Superhydrophobic Coating for Efficient Microplastic Removal. *Coatings* **2021**, *11*, 1258. https://doi.org/10.3390/coatings11101258

Academic Editor: Kui Cheng

Received: 16 September 2021
Accepted: 13 October 2021
Published: 16 October 2021

1. Introduction

The presence of solid pollutants such as microplastics (MPs) is a concerning issue around the globe that will affect the economy, the quality of food and soils, and the health of animals and the human population. MPs are smaller than 5 mm in size and present a wide variety of morphologies such as rounded and irregular shapes or fibers. Their chemical composition also varies and they can be polypropylene (PP), polystyrene (PS), polyethylene (PE), or copolymers such as nylon. Additionally, MPs can cause several types of health problems, such as neurotoxicity and disruption of immune functions, and they have even been reported to translocate to the circulatory system [1–3].

To remove MPs from water and avoid future issues, different technologies have been used such as electrocoagulation, filtration membranes and air flotation, among others [4,5]. Despite the fact that these methods present high separation efficiencies, they also have limitations such as fouling of the whole surface or even causing MPs to fragment into nanoplastics [6,7]. Therefore, it is necessary to study different materials that can remove MPs without affecting their size and causing surface contamination. In this scenario, and apart from the previously cited methods, the wettability of MPs should be considered. Due to the organic nature and presence of carbon-carbon or even carbon-halogen bonds, the surface free energy of the polymers tends to be low, which decreases the wetting properties. Therefore, the surface free energy of different materials plays a key role in the removal of MPs. Superhydrophobic materials are surfaces with extremely high water contact angles (WCA > 150°), low sliding angles (SA < 10°), and low contact angle hysteresis (CAH < 10°), thereby showing water repellency [8]. Moreover, it is well known that these materials

also present superoleophilic properties and underwater superoleophilicity, with oil contact angles (OCA) and underwater oil contact angles (UWOCA) lower than 10° [9–11]. Superhydrophobic materials have been used in a wide variety of applications such as in corrosion resistance [12,13], photodegradation of pollutants [14,15], self-cleaning [16,17], anti-biofouling [18,19], anti-icing [20,21], distillation [22,23], oil/water separation [24–26], and ethanol/water separation [27,28]. Despite the fact that these materials can remove miscible or immiscible pollutants, the separation of solid pollutants from water still remains a challenge. Additionally, the use of ceramic particles such as SiO_2, Al_2O_3, or TiO_2 increases the roughness of the surface, which is a key point for superhydrophobic surfaces, leading to the heterogeneous Cassie-Baxter wetting state as well as increasing the durability of the coating itself [29–31].

Herein, we present a composite superhydrophobic coating made of zinc laurate and TiO_2 particles that was obtained by combining electrodeposition and electrophoresis. The coating has a WCA of 153° and an OCA of 0°. It also presents excellent durability against abrasion due to the presence of TiO_2 particles. Taking advantage of the water repellency of the surface and its high affinity for hexane, we observed that MPs migrate from the water to hexane due to their affinity for the organic phase. As a result, this process promotes the removal of high-density polyethylene (HDPE) MPs with efficiencies close to 100%. This application provides a new way of using superhydrophobic surfaces in the removal of solid pollutants based on their wetting properties.

2. Experimental Procedure

2.1. Fabrication

The following method was used to deposit a superhydrophobic coating onto a pure aluminum substrate. Cleaned plates of UNS A91070 aluminum (99.999%) were grinded manually and vertically with P1200 SiC abrasive paper. A solution of 0.1 M lauric acid, 0.05 M $ZnCl_2$ and 1 g/L of TiO_2 with a particle diameter of 0.2 ± 0.04 µm (purchased from Scharlau, Acros Organics and Alfa Aesar, respectively) was prepared in analytical grade ethanol (purchased from Scharlau), with the corresponding suspension obtained after stirring. Two aluminum plates acting as electrodes were immersed vertically and separated 2 cm from each other in the solution. Finally, a current density of 0.02 A/dm^2 was applied for 900 s. After that, the samples were removed from the electrolytic solution, cleaned with ethanol, and dried in air. Samples were obtained as mentioned above and the experimental conditions such as temperature (25 °C), reactant concentrations and the potential were controlled constantly. A coating was formed on the aluminum substrate, covering the surface.

2.2. Characterization Techniques

To understand the roles of the reactants and morphology, different characterization techniques were used to determine morphology and the chemical composition. The sample surface was characterized on a JEOL J-7100 field emission scanning electron microscope (FESEM, JEOL Ltd., Tokyo, Japan) to study the morphology in detail. Energy-dispersive X-ray Spectroscopy (EDS, Oxford Instruments, Oxfordshire, UK) microanalysis was used to determine the semiquantitative elemental composition of the generated coatings (samples were carbon sputtered to enhance observation). The study of the surface nanostructure was performed with a transmission electron microscope. High-resolution transmission electron microscopy (HRTEM, JEOL Ltd., Tokyo, Japan) was conducted with a JEOL JEM 2100 microscope coupled to an EDS detector and the Selected Area Electron Diffraction (SAED); the samples were supported on a holy carbon film on a copper grid. The Gatan 1.7 and CaRIne 4.0 software programs were used to determine the interplanar distances and planes. High-resolution X-ray photoelectron spectroscopy (HR-XPS) was performed on a PHI ESCA-5500 system (PHI, Chanhassen, MN, USA) using a monochromatic X-ray source (Kα(Al) = 1486.6 eV and 350 W) to determine the chemical composition of the system. Infrared spectroscopy was also used to establish the presence of hydrocarbon acid

and its chemical bonds. For this purpose, attenuated total reflectance-Fourier transform infrared spectroscopy (ATR-FTIR) in the range of 4000–525 cm^{-1} at a resolution of 4 cm^{-1} was performed on an ABB Bomem FTLA spectrometer (Québec, QC, Canada). X-ray diffraction (XRD) was mainly used to determine the structure of the alumina powder, using a PANalytical X'Pert PRO MPD Alpha1 powder diffractometer (PANalytical, Lelyweg, The Netherlands) in the Bragg-Brentano θ/2θ geometry with a radius of 240 mm and Cu Kα1 radiation (λ = 1.5406 Å). Images of the static WCA, CAH and SA were taken using a sessile method involving a Levenhuk digital microscope and 3.5 µL of deionized (DI) water at room temperature. Hexane (purchased from Panreac) was used to measure the OCA. In the case of HDPE-MPs, the contact angle measurements were performed as follows: MPs were sprinkled onto a glass slide containing an adhesive before being flattened by another glass slide to prevent roughness effects, with the excess powder removed. The ImageJ software version 1.53 m was used to measure all contact angles. The values reported are the average of three measurements of droplets at different parts on the surface.

2.3. Durability Test

The abrasive grinding paper test was used to determine surface durability in severe abrasive conditions. The superhydrophobic surface (10 mm × 40 mm × 1 mm) was placed in contact with P1200 SiC grinding paper and moved 10 cm across it for 10 cycles while a constant load of 5 kPa was applied. After each cycle, the surface was cleaned with forced air to remove the TiO_2 powder before measuring the WCA and SA to determine the robustness of the surface.

2.4. Microplastics

To remove MPs from water, 3.5 wt% NaCl aqueous solution in DI water (pH 7) was prepared with 30 mg of HDPE-MP measuring 133 ± 34 µm (purchased from Abifor) in 30 mL of aqueous solution. Hexane (up to 150 µL) was carefully poured under constant stirring until the MPs moved to the organic phase. After that, the superhydrophobic surface was moved towards the hexane droplet containing the MPs. This process was repeated with the same sample until the MPs were no longer observable and had all been removed. The superhydrophobic surface was then cleaned with ethanol to remove the pollutants. To quantify the number of MPs removed, the mass of MPs on the superhydrophobic surface was weighed on a laboratory balance. A Zeiss Axiovert 100A Inverted Microscope with white light was used to study the size distribution of the MPs by measuring the size of 200 MPs from different images and determining their sizes with ImageJ. Oil Red O (Scharlab) was used to dye the organic solvent.

3. Results and Discussion

3.1. Morphology

The coating surface morphology was studied by FESEM and is shown in Figure 1a–c after 900 s of the electrodeposition-electrophoresis process. As can be seen, the coating displayed a flower-like structure, with the TiO_2 particles located at the inner parts of the micro-flowers and also partially covering their surface (Figure 1a). Moreover, a closer look at the structure revealed a group of randomly-organized layers (Figure 1b) with a thickness of 70 nm (Figure 1c). EDS microanalysis was used to determine the elemental composition of the micro-flower particles. As shown in Figure 1d, the micro-flowers contained Zn (Kα = 8.630 eV and Lα = 1.012 eV) and O (Kα = 0.525 eV). The Al signal (Kα = 1.484 eV) corresponded to the aluminum substrate and there was also a signal corresponding to the presence of Ti (Kα = 4.508 eV and Lα = 0.452 eV). Additionally, the high C peak (Kα = 0.277 eV) was due to the carbon sputtering of the samples and the lauric acid. HRTEM enabled the observation of the structure at the nanometer scale. The structure observed corresponded to a unit (petal) of the flower-like morphology and was composed of thin layers overlapping one another (Figure 1e).

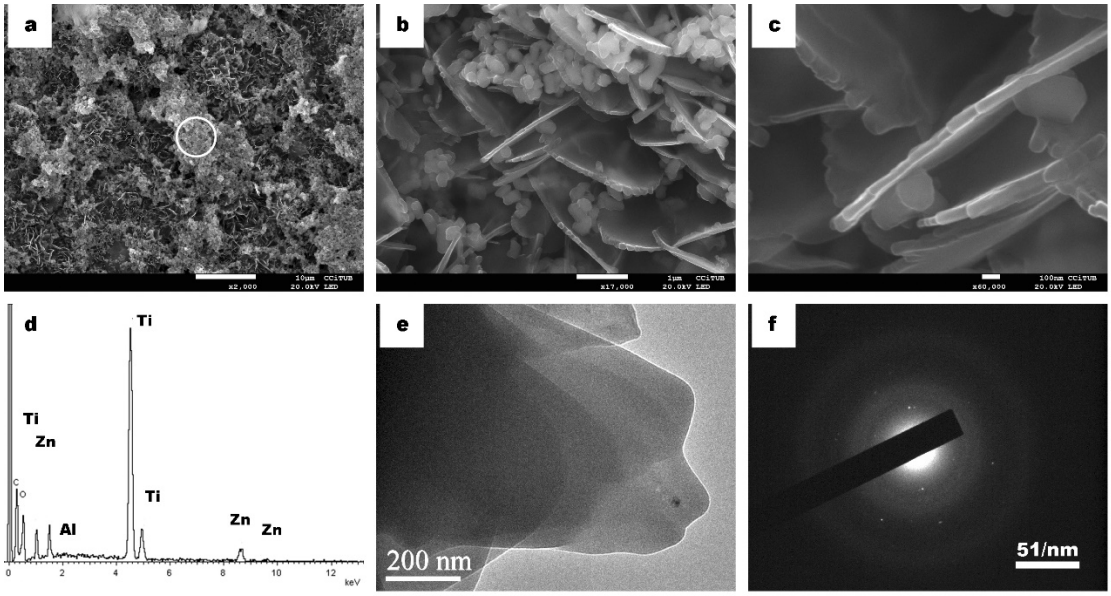

Figure 1. FESEM images of the superhydrophobic coating after 900 s of the electrodeposition -electrophoresis process at different magnifications showing (**a**) TiO_2 particles accumulated at the top of the flower-like structure, (**b**) TiO_2 particles and intercalation between the petals, and (**c**) the corresponding nanostructured petal. (**d**) EDS analysis of the flower-like structure, (**e**) an HRTEM micrograph of the petals from the flower-like structure, and (**f**) the SAED pattern showing weak rings from the petal.

Electron microscopy characterization revealed that the surface was composed of a microstructure, corresponding to the flower-like structure with the presence of TiO_2 particles, and a nanostructure of the same flower-like structure, corresponding to thin layers overlapping one another. This combined morphology and their level of structure produced a hierarchical structure that is a key point in the superhydrophobic properties of the coating. In fact, the method used to obtain the superhydrophobic coating involved two different processes: electrodeposition (EDP), also known as electroplating, and electrophoresis (EPD) [32]. EDP is based on the Faradaic process where ionic species from the ethanol solution consisting of $ZnCl_2$ deposits under certain voltages. Meanwhile, during EPD, TiO_2 particles in suspension migrate from the solution to the aluminum (acting as a cathode) via electrophoresis and convective diffusion.

3.2. Chemical Composition

To determine the chemical composition of the coating and the main chemical compound that decreases the surface free energy of the system, three different characterization techniques were used: XRD to identify the phases present in the surface, and ATR-FTIR and HR-XPS to reveal the surface chemistry of the coating.

XRD showed the presence of two different phases assigned to the aluminum substrate (bcc crystal structure), corresponding to the 2θ positions and planes 38.4° (111), 45.7° (200), 65.1° (220), 78.2° (311) and 82.4° (222), and to the rutile phase of TiO_2 in a tetragonal crystal structure, corresponding to the 2θ positions and planes 27.4° (110), 36.0° (101), 41.2° (111) and 54.3° (211) (Figure 2a). Additionally, a group of peaks between 2θ 10° and 30° was observed in the diffractogram (Figure 2b). The most intense one at 27.4° was previously assigned to the TiO_2 phase, but there were also five different peaks corresponding to zinc laurate as a quasi-crystalline phase.

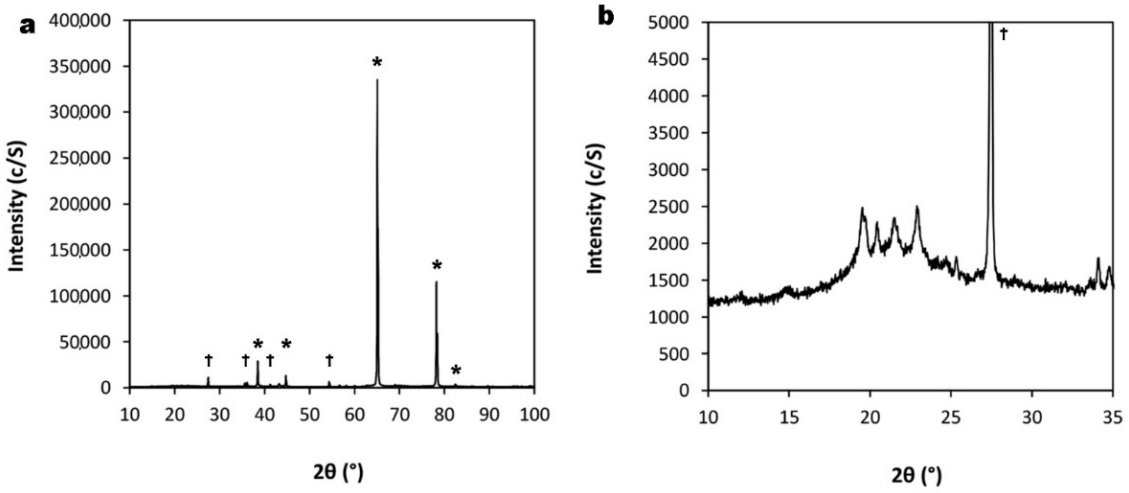

Figure 2. (**a**) XRD of the coating after 900 s of EDP, revealing two phases assigned to the Al (*) substrate and TiO_2 (†). (**b**) Detailed area of the XRD showing the quasi-crystalline phase assigned to zinc laurate.

Figure 3 shows the ATR-FTIR spectra of both the coating produced and pure lauric acid. Different symbols were used to denote the vibrations, with δ used for bending, σ for rocking, ν for stretching, and τ for twisting. Pure lauric acid was characterized, with the most characteristic bands related to the carboxyl group or the carbon chain [33–35]. It is important to note the presence of a broad band between 3000 cm^{-1} and 2500 cm^{-1}, which was assigned to the carboxyl group of lauric acid. For the carbonyl group, a band at ca. 1689 cm^{-1} was assigned to νC=O and the one at ca. 1298 cm^{-1} was assigned to νC–O. For the carbon chain, bands appearing at ca. 2951 cm^{-1}, ca. 2911 cm^{-1} and ca. 2845 cm^{-1} corresponded to alkyl chain stretching and were assigned to $\nu_{as}CH_3$, $\nu_{as}CH_2$ and ν_sCH_2–CH_2, respectively. The bands located at ca. 1298 cm^{-1} and ca. 1192 cm^{-1} were assigned to νO–H. A band at ca. 1082 cm^{-1} corresponded to σCH_3, while the two different bands found below 1000 cm^{-1} were identified at ca. 934 cm^{-1} and were assigned to δO–H. Finally, the band at ca. 776 cm^{-1} corresponded to δC-H out of plane. The ATR-FTIR spectrum of the coating was very similar to that of pure lauric acid [33–37]. However, the absence of the broad band between 3000 cm^{-1} and 2500 cm^{-1} was significant and indicated the formation of a new bond given the absence of the carboxylic group. There were three strong bands in the spectrum for the coating, such as that for lauric acid, located at ca. 2951 cm^{-1}, ca. 2914 cm^{-1} and ca. 2846 cm^{-1} that corresponded to $\nu_{as}CH_3$, $\nu_{as}CH_2$ and ν_sCH_2–CH_2, respectively. A weak band at ca. 1584 cm^{-1} was attributed to $\nu_{as}COO$, a strong band at ca. 1533 cm^{-1} was associated with $\nu_{as}COO$ and a band with medium intensity at ca. 1400 cm^{-1} was assigned to ν_sCOO. A strong band at ca. 1455 cm^{-1} was attributed to δCH_2. A medium band at ca. 1081 cm^{-1} was related to τCH_3, while another one at ca. 716 cm^{-1} was assigned to δCH_2. An important difference between the spectrum for the superhydrophobic coating and that for lauric acid was the presence of the broad band with low transmittance at ca. 3460 cm^{-1} that were assigned to the –OH and H–O–H bonds [38]. Moreover, a group of bands between ca. 1000 cm^{-1} and ca. 525 cm^{-1} was assigned to the presence of TiO_2. The band at ca. 1081 cm^{-1} was assigned to Ti–O–H deformation, while the broad band at ca. 600 cm^{-1} was assigned to the O–Ti–O bond in the TiO_2 lattice [39,40].

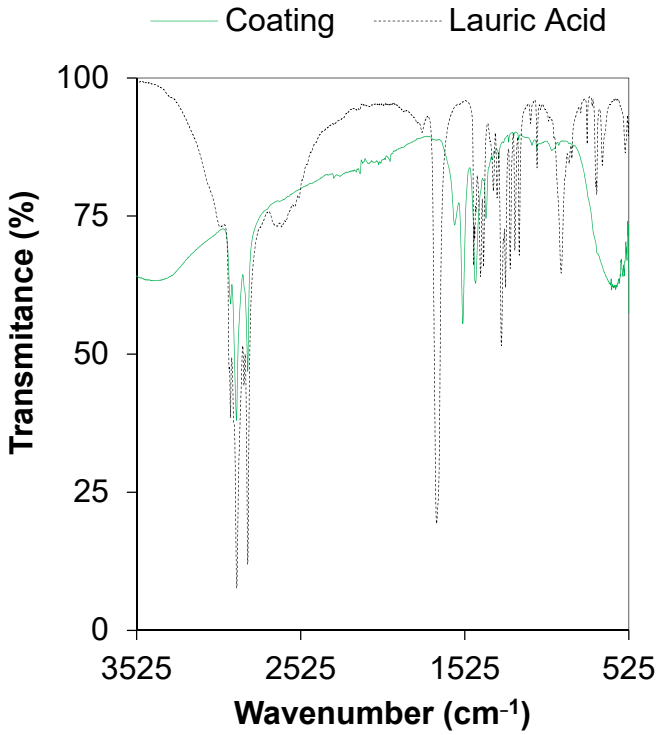

Figure 3. ATR-FTIR spectra of pure lauric acid (dotted line) and the coating (solid line) revealing the presence of a carboxylate functional group assigned to zinc laurate.

HR-XPS was applied to determine the chemical composition of the coating at the surface level, considering the five different elements present in the sample. Al-2p revealed the presence of two deconvolutions at 74 eV and 81 eV that were assigned to Al-O bonds from the thick alumina layer from the aluminum substrate (Figure 4a) [41]. For C-1s, there were three deconvolutions: one at 284 eV corresponding to the C–C bond, one at 285 eV assigned to the carbonyl group (C=O) and one at 288 eV assigned to the carboxylate group (COO^{-}) (Figure 4c) [42]. In the case of Ti-2p, there were two deconvolutions at 458 eV and 464 eV assigned to the Ti–O bond from TiO_2 and its satellite Ti 2p1/2, respectively (Figure 4d) [43]. For the O-1s signal, there were three deconvolutions: one at 529 eV from the Zn–O bond, one at 530 eV from TiO_2 and one at 531 eV assigned to COO–Zn (Figure 4e) [44,45]. Finally, for Zn-2p, there was only one deconvolution at 1021 eV assigned to Zn (II) combined with an OH group, as in $Zn(OH)_2$ (Figure 4f) [44].

XRD, ATR-FTIR, and HR-XPS allowed us to identify the chemical composition achieved after the EDP/EPD processes. XRD showed that the coating was made of TiO_2 particles that covered the upper layers of the surface and it also revealed the presence of a quasi-crystalline phase. ATR-FTIR and HR-XPS revealed and confirmed that zinc laurate ($Zn(C_{11}H_{20}COO)_2$) was the main compound of the surface that contributes to decreasing the surface free energy of the coating due to the presence of the alkyl chain. This, combined with the hierarchical structure that increases the roughness of the system, endows the coating with superhydrophobic properties.

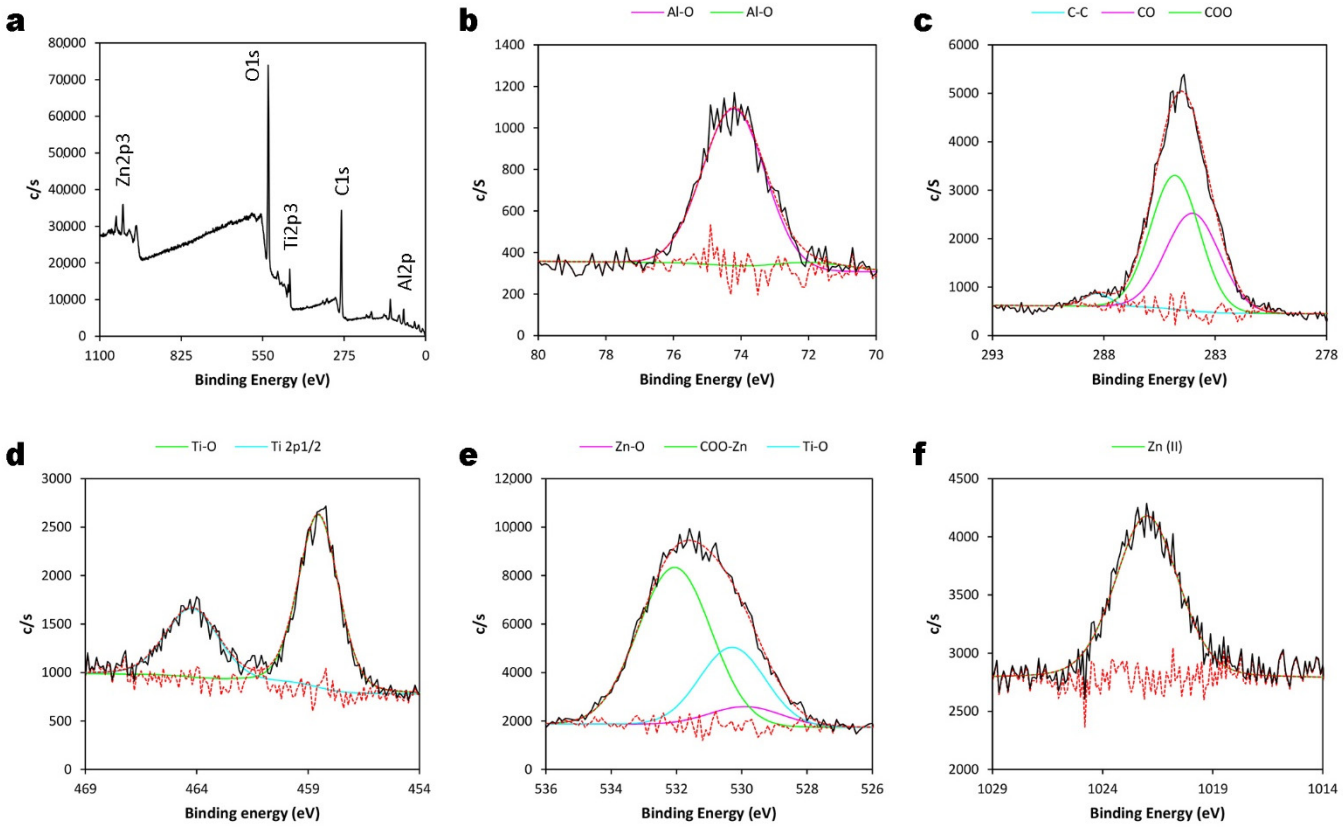

Figure 4. (**a**) General XPS spectrum of the superhydrophobic surface. The HR-XPS spectra of (**b**) Al-2p, (**c**) C-1s, (**d**) Ti-2p, (**e**) O-1s, and (**f**) Zn-2p, revealing the presence of zinc laurate as the main compound of the coating as well as the presence of TiO_2.

3.3. Wetting Properties

Wettability is a key parameter for defining superhydrophobic properties. Therefore, it is necessary to measure the WCA, CAH, SA, and OCA. The UNS A91070 aluminum substrate showed a WCA of $92 \pm 3°$, corresponding to a hydrophobic state (Figure 5a). After 900 s of EDP, the coating obtained had a WCA of $153 \pm 1°$, a CAH of $1 \pm 1°$ and an SA of $1 \pm 1°$, indicating superhydrophobicity (Figure 5b) and self-cleaning properties, with both occurring as a consequence of the Cassie-Baxter wetting state [46]. Moreover, to determine the ability to separate oil from water for the removal of MPs from the aqueous phase, the OCA was also measured, which showed a value of 0°, revealing superoleophilicity due to the instant sorption of hexane throughout the whole structure (Figure 5c). Additionally, the WCA and OCA of the HDPE-MP were measured as these are also defining parameters in the ability of superhydrophobic materials to remove solid pollutants. The WCA of the HDPE-MP was $136 \pm 1°$ (Figure 5d) and the OCA was 0°, with instant oil sorption (Figure 5e).

The WCA and OCA values showed that the coating presented extremely high water repellency and a higher affinity for hexane compared to water, while the MPs presented hydrophobic characteristics and a higher affinity for hexane than for water. Based on this affinity of the HDPE-MPs and the superhydrophobic coating for the oleophilic state, the system was used to separate MPs.

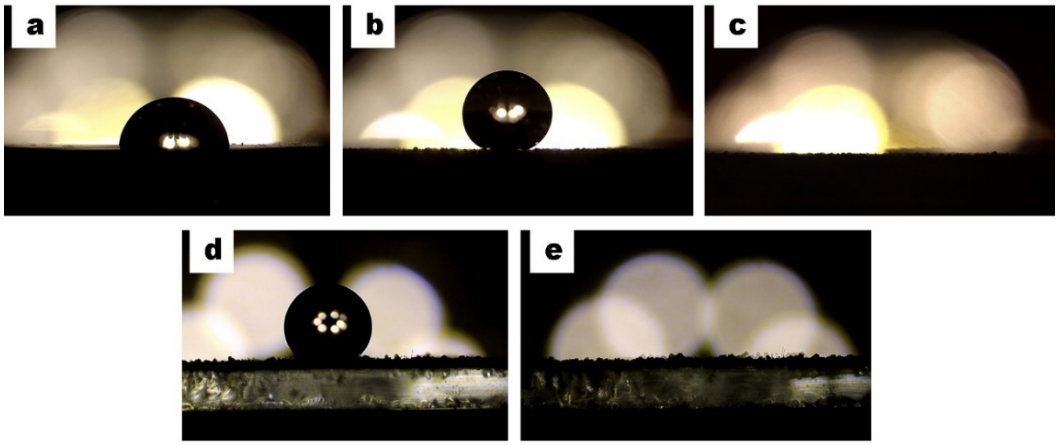

Figure 5. Contact angle measurements: (**a**) WCA on the aluminum substrate (93 ± 3°), (**b**) WCA on the superhydrophobic coating (153 ± 1°), (**c**) OCA on the superhydrophobic coating (0°), (**d**) WCA on the MP (136 ± 1°), and (**e**) OCA on the HDPE-MP (0°).

3.4. Durability

The robustness of superhydrophobic materials have to be studied to determine and understand the mechanisms that decrease their wettable properties and to establish the different ways of improving their resistance to abrasive environments. We carried out the abrasive paper test to determine the durability of the superhydrophobic coating obtained in this study. Figure 6a depicts how the WCA and SA changed slightly after 10 cycles (100 cm) of the abrasive test under 5 kPa. Before the test, the WCA was 152° and decreased to 150°, while the SA increased from 1° to nearly 6°, revealing that despite the abrasion, the surface also presented self-cleaning and low adhesion properties. In fact, in the first cycle of the abrasion test, TiO_2 particles were found on the sandpaper. Despite this, the surface was still superhydrophobic after subsequent cycles. As depicted in Figure 6b, superficial TiO_2 particles were no longer observed due to their detachment from the upper layers of the coating, but they remained present between the petals of the flower-like structure and also in the lower parts of the coating that were not in contact with the abrasive paper. Moreover, the nanostructures were still present throughout the coating.

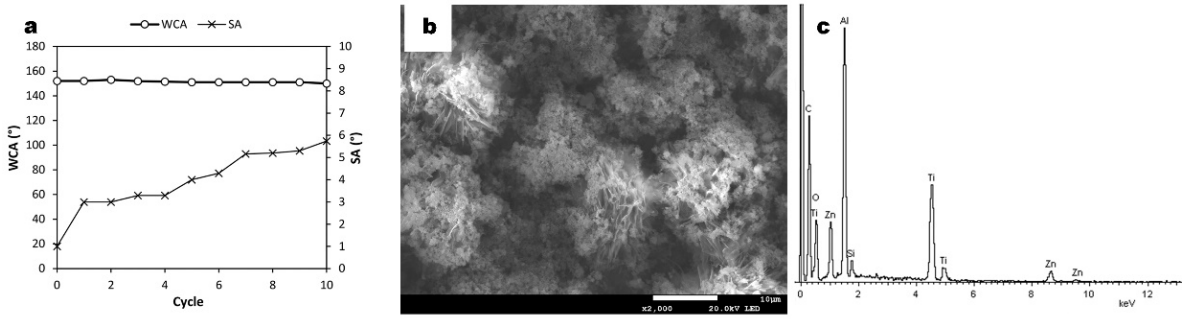

Figure 6. Durability test using P1200 SiC abrasive paper, which revealed that the surface was still superhydrophobic after 10 cycles: (**a**) the WCA remains higher than 150° and the SA is lower than 10°; (**b**) FESEM image of the surface after the test showing the presence of TiO_2 as well as the flower-like structure and (**c**) EDS showing the presence of TiO_2.

These results could be explained by considering two different mechanisms. Firstly, as the coating remained superhydrophobic after the test, this revealed that there were no pinning sites introduced during the abrasion. Thus, the superhydrophobic coating was remarkably homogeneous in its chemical composition and the zinc laurate was not severely affected by the abrasion. Secondly, TiO_2 particles from the upper layers of the coating were removed first, leading to increased durability and the retention of superhydrophobic properties after each abrasive cycle. Despite the fact that the WCA remained more or less

constant during the whole test, the SA changed, indicating an increase in water droplet adherence to the surface. The changes in the SA can be divided into four steps: those observed in the first cycle, then from the second to the fourth cycle, then up to the seventh cycle and finally up to the 10th cycle. The first cycle was characterized by the removal of the upper layers of the superhydrophobic coating, which were the TiO_2 particles, explaining the increase in the SA from 1° to 3°. In the second cycle, the SA remained at a slight plateau since the layers underneath the TiO_2 were chemically homogeneous and presented a low surface free energy, which led to the maintenance of its low adherence properties. Then, in the third cycle, the SA increased to 5.5° since the chemically homogenous structure that was the flower-like structure had become slightly damaged by the abrasive paper. Finally, in the fourth cycle, the SA again plateaued due to the presence of a chemically homogenous structure.

The durability of the superhydrophobic coating and the absence of pinning sites after the abrasive paper test were due to the presence of TiO_2 particles as well as the hierarchical structure [47–49]. The TiO_2 particles prevented the degradation of the hierarchical structures during the early stages. After their removal by the abrasive paper, the flower-like structure was highly homogenous in its chemical composition, promoting low water adherence to the coating itself and maintaining its superhydrophobic properties.

3.5. Microplastics

It is well known that superhydrophobic materials and surfaces can separate oil from water as well as their stabilized emulsions (o/w) [50–52]. Taking advantage of this ability, we used the superhydrophobic material obtained in this study to remove MPs from water. In this section, we report how MPs move from the aqueous phase to the organic one and are captured and removed by the superhydrophobic surface. Samples of the superhydrophobic surface were used to remove MPs from water. Hexane was used as the oil phase due to its density (0.659 g/mL at 25 °C). As shown before, HDPE-MPs present an OCA of 0°, indicating a greater affinity for hexane than for water (WCA = 136°). Moreover, oil droplets containing the MPs will float due to the low density of hexane. Firstly, the aqueous solution contained 30 mg of HDPE-MP (Figure 7a). In the first removal step, the superhydrophobic surface was able to capture 15 mg of the HDPE-MP from the oil droplet over 10 s (Figure 7b). After that, there were still some MPs present in the oil droplet. Thus, the superhydrophobic surface was used again to capture the remaining MPs, removing 8 mg of HDPE-MP after 6 s. However, there were still a few MPs present; therefore, the process was repeated for a third time and 7 mg were removed over 2 s, leaving a clear aqueous solution behind without any evidence of MPs and with the hexane completely removed (Figure 7c). After each removal step, the oil droplet decreased in volume since the surface also adsorbed some of the hexane due to its superhydrophobic/superoleophilic properties. At the end of each step, a water droplet could easily slide over the whole surface, removing the adhering MPs due to its self-cleaning properties that prevented surface fouling. The removal process was repeated up to 12 times without the surface losing its superhydrophobic properties, repeatedly allowing the removal of MPs. These results demonstrated the strong ability of the surface to remove MPs from water and also its reusability. Additionally, the MP removal ability of the superhydrophobic coating was compared with that of the bare aluminum substrate, which was not able to remove MPs. This can be explained by the fact that the bare aluminum substrate is hydrophobic (WCA = 93°), whereas the superhydrophobic surface can adsorb oil. Thus, it is necessary to modify the surface free energy, which was achieved in this study with zinc laurate that conferred superhydrophobicity and underwater superoleophilicity. The MP removal ability of the superhydrophobic surface was also compared with that of a control sample where no hexane was used. Due to the extreme water repellency of the surface, the MPs did not move from the aqueous phase to the surface, revealing that an organic phase such as an oil is necessary to remove solid pollutants such as MPs.

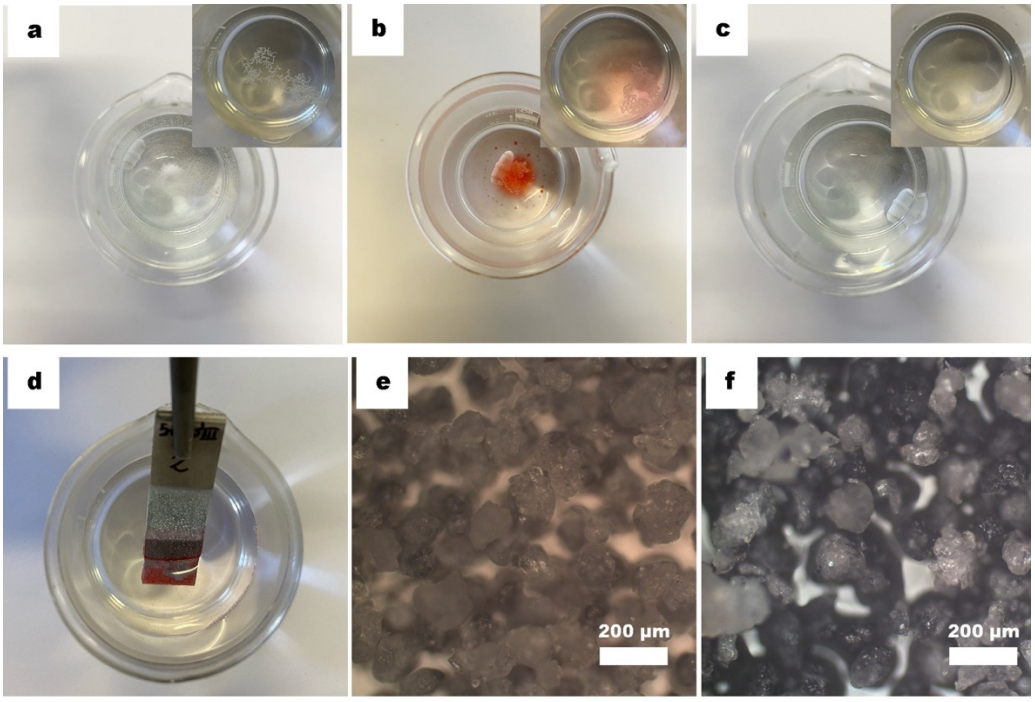

Figure 7. Three different steps to completely remove the MPs from water, with the insets showing the HDPE-MP powder: (**a**) aqueous solution containing 30 mg of HDPE-MP; (**b**) after stirring, the MPs migrated to the organic phase (in red, Oil Red O); (**c**) the solution without any MP or hexane; (**d**) the superhydrophobic coating removing the organic phase containing the HDPE-MP powder; (**e**) HDPE-MPs before the removal process; and (**f**) after the process, with no changes in their morphology and size.

The removal efficiency of the process can be calculated as follows (Equation (1)):

$$\xi\ \% = M_{MP}/M_{0,MP} \times 100 \quad (1)$$

where $M_{0,MP}$ and M_{MP} are the mass of the HDPE-MPs before and after the removal process, respectively. Thus, the overall removal efficiency was higher than 99%, with 0.2 mg/µL of HDPE-MPs removed per volume of hexane. Additionally, the HDPE-MP size was not affected by the removal process as its sizes were 133 ± 34 µm and 133 ± 33 µm before and after each removal step, respectively (Figure 7d,e). Furthermore, HDPE-MPs did not dissolve or swell. These characteristics are especially important since some treatment methods, such as those using membranes, usually lead to MPs breaking down into smaller particles under the water pressure, which limits their application.

As shown before, superhydrophobic surfaces can remove MPs from water as a result of their superwettable properties. As the contact angle measurements revealed, MPs present a higher affinity for hexane (OCA = 0°) than for water (WCA = 136°), while the superhydrophobic surface behaves in slightly the same manner, presenting more affinity for hexane (OCA = 0°) than for water (WCA = 153°).

Considering the results, it is of interest to determine the mechanism of MP removal. As shown above, the MPs were initially randomly distributed in the aqueous phase. Under stirring conditions and due to the low affinity for water, they were displaced to the center of the stirring vortex, into which 150 µL of hexane were added. Herein, the MPs migrated from the water to hexane due to the repellency to water and their higher affinity for hexane. The oil containing the MPs was then adsorbed by the superhydrophobic surface when it was moved towards the pollutants due to the superoleophilic properties of the surface.

Herein, we show that superhydrophobic coatings can also be used in an innovative way to address the increasingly significant issue of pollution caused by MPs [53]. The coating obtained in this study confirmed that the wetting properties of superhydrophobic

surfaces combined with the properties of MPs can be used to remove these pollutants [54]. Further research is needed to clearly determine the physico-chemical mechanisms that lead to MPs migrating from water to oil, as well as the effects of the oil used and the different morphologies and systems in the removal of MPs from oceans, rivers and water treatment plants.

4. Conclusions

A superhydrophobic coating with a static WCA of 153°, an SA of 1, and a CAH of 1° was achieved by combining electrodeposition and electrophoresis. Its chemical composition consisted of zinc laurate hierarchical structures as well as TiO_2 particles. Additionally, its durability was studied in an abrasive paper test. After 100 cm of abrasion with the P1200 SiC abrasive paper, the surface was still superhydrophobic, indicating that the surface was chemically homogeneous and enhanced by the presence of TiO_2 particles located at the upper layers of the coating. Finally, taking advantage of its superhydrophobic/superoleophilic properties, the coating was used to remove HDPE-MPs by moving it towards the oil droplet containing the MPs. This method had an efficiency higher than 99% and did not lead to the MPs breaking down. The migration of MPs from water to the organic phase combined with the superwettable properties of the surface allowed the removal of these solid pollutants from water. Therefore, a simple and straightforward method to remove MPs using superhydrophobic surfaces was carried out, providing a new way of studying and understanding superhydrophobic materials in the removal of solid pollutants in water treatment plants and their environmental applications.

Author Contributions: Conceptualization, O.R.-A.; methodology, O.R.-A. and A.B.-T.; software, O.R.-A. and A.B.-T.; validation, O.R.-A., A.B.-T. and N.L.-I.; formal analysis, O.R.-A. and A.B.-T.; investigation, O.R.-A. and A.B.-T.; resources, N.L.-I.; data curation, O.R.-A. and A.B.-T.; writing—original draft preparation, O.R.-A. and A.B.-T.; writing—review and editing, O.R.-A. and A.B.-T.; visualization, O.R.-A.; supervision, O.R.-A., A.B.-T. and N.L.-I. All authors have read and agreed to the published version of the manuscript.

Funding: This research received no external funding.

Data Availability Statement: Data sharing not applicable.

Conflicts of Interest: The authors declare no conflict of interest.

References

1. Zhou, R.; Lu, G.; Yan, Z.; Jiang, R.; Bao, X.; Lu, P. A review of the influences of microplastics on toxicity and transgenerational effects of pharmaceutical and personal care products in aquatic environment. *Sci. Total Environ.* **2020**, *732*, 139222. [CrossRef] [PubMed]
2. Prata, J.C.; da Costa, J.P.; Lopes, I.; Duarte, A.C.; Rocha-Santos, T. Environmental exposure to microplastics: An overview on possible human health effects. *Sci. Total Environ.* **2020**, *702*, 134455. [CrossRef] [PubMed]
3. Teles, M.; Balasch, J.C.; Oliveira, M.; Sardans, J.; Peñuelas, J. Insights into nanoplastics effects on human health. *Sci. Bull.* **2020**, *65*, 1966–1969. [CrossRef]
4. Estahbanati, M.R.K.; Kiendrebeogo, M.; Mostafazadeh, A.K.; Drogui, P.; Tyagi, R.D. Treatment processes for microplastics and nanoplastics in waters: State-of-the-art review. *Mar. Pollut. Bull.* **2021**, *168*, 112374. [CrossRef]
5. Enfrin, M.; Dumée, L.F.; Lee, J. Nano/microplastics in water and wastewater treatment processes—Origin, impact and potential solutions. *Water Res.* **2019**, *161*, 621–638. [CrossRef]
6. da Costa, J.P.; Santos, P.S.M.; Duarte, A.C.; Rocha-Santos, T. (Nano)plastics in the environment—Sources, fates and effects. *Sci. Total Environ.* **2016**, *566–567*, 15–26. [CrossRef]
7. Chen, Z.; Liu, J.; Chen, C.; Huang, Z. Sedimentation of nanoplastics from water with Ca/Al dual flocculants: Characterization, interface reaction, effects of pH and ion ratios. *Chemosphere* **2020**, *252*, 126450. [CrossRef]
8. Bhushan, B.; Jung, Y.C. Natural and biomimetic artificial surfaces for superhydrophobicity, self-cleaning, low adhesion, and drag reduction. *Prog. Mater. Sci.* **2011**, *56*, 1–108. [CrossRef]
9. Su, B.; Tian, Y.; Jiang, L. Bioinspired interfaces with superwettability: From materials to chemistry. *J. Am. Chem. Soc.* **2016**, *138*, 1727–1748. [CrossRef] [PubMed]
10. Liu, M.; Wang, S.; Jiang, L. Nature-inspired superwettability systems. *Nat. Rev. Mater.* **2017**, *2*, 17036. [CrossRef]

11. Chu, Z.; Feng, Y.; Seeger, S. Oil/Water separation with selective superantiwetting/superwetting surface materials. *Angew. Chemie Int. Ed.* **2015**, *54*, 2328–2338. [CrossRef] [PubMed]
12. Miao, Y.; Zhang, D.; Cao, N.; Yang, L.; Ju, H.; Boukherroub, R.; Lin, X.; Li, H.; Jin, Y. Mussel-inspired superhydrophobic surfaces on 316L stainless steel with enhanced corrosion resistance. *Metall. Mater. Trans. A* **2020**, *51*, 909–919. [CrossRef]
13. Li, J.; Li, J.; Liu, Y.; Wen, Y.; Jiang, J.; Shang, W.; Peng, N. Corrosion resistance and forming mechanism of the lauric acid/graphene composite films on aluminum alloy by electrodeposition. *Adv. Eng. Mater.* **2021**, 2001540. [CrossRef]
14. Baig, U.; Matin, A.; Gondal, M.A.; Zubair, S.M. Facile fabrication of superhydrophobic, superoleophilic photocatalytic membrane for efficient oil-water separation and removal of hazardous organic pollutants. *J. Clean. Prod.* **2019**, *208*, 904–915. [CrossRef]
15. Ge, B.; Tang, S.; Zhang, H.; Li, W.; Wang, M.; Ren, G.; Zhang, Z. Water vapor recovery device designed with interface local heating principle and its application in clean water production. *J. Mater. Chem. A* **2021**, *9*, 7967–7976. [CrossRef]
16. Luo, J.; Wang, L.; Huang, X.; Li, B.; Guo, Z.; Song, X.; Lin, L.; Tang, L.-C.; Xue, H.; Gao, J. Mechanically durable, highly conductive, and anticorrosive composite fabrics with excellent self-cleaning performance for high-efficiency electromagnetic interference shielding. *ACS Appl. Mater. Interfaces* **2019**, *11*, 10883–10894. [CrossRef]
17. Wang, M.; Zi, Y.; Zhu, J.; Huang, W.; Zhang, Z.; Zhang, H. Construction of super-hydrophobic PDMS@MOF@Cu mesh for reduced drag, anti-fouling and self-cleaning towards marine vehicle applications. *Chem. Eng. J.* **2021**, *417*, 129265. [CrossRef]
18. Zhang, B.; Li, J.; Zhao, X.; Hu, X.; Yang, L.; Wang, N.; Li, Y.; Hou, B. Biomimetic one step fabrication of manganese stearate superhydrophobic surface as an efficient barrier against marine corrosion and Chlorella vulgaris-induced biofouling. *Chem. Eng. J.* **2016**, *306*, 441–451. [CrossRef]
19. Kumaravel, V.; Nair, K.M.; Mathew, S.; Bartlett, J.; Kennedy, J.E.; Manning, H.G.; Whelan, B.J.; Leyland, N.S.; Pillai, S.C. Antimicrobial TiO2 nanocomposite coatings for surfaces, dental and orthopaedic implants. *Chem. Eng. J.* **2021**, *416*, 129071. [CrossRef]
20. Zhang, J.; Gu, C.; Tu, J. Robust slippery coating with superior corrosion resistance and anti-icing performance for AZ31B Mg alloy protection. *ACS Appl. Mater. Interfaces* **2017**, *9*, 11247–11257. [CrossRef]
21. Rico, V.; Mora, J.; García, P.; Agüero, A.; Borrás, A.; González-Elipe, A.R.; López-Santos, C. Robust anti-icing superhydrophobic aluminum alloy surfaces by grafting fluorocarbon molecular chains. *Appl. Mater. Today* **2020**, *21*, 100815. [CrossRef]
22. Zhang, W.; Hu, B.; Wang, Z.; Li, B. Fabrication of omniphobic PVDF composite membrane with dual-scale hierarchical structure via chemical bonding for robust membrane distillation. *J. Memb. Sci.* **2021**, *622*, 119038. [CrossRef]
23. Abdu, B.; Munirasu, S.; Kallem, P.; Hasan, S.W.; Banat, F. Investigating the effect of various foulants on the performance of intrinsically superhydrophobic polyvinylidene fluoride membranes for direct contact membrane distillation. *Sep. Purif. Technol.* **2020**, *252*, 117416. [CrossRef]
24. Shi, Y.; Hu, Y.; Shen, J.; Guo, S. Optimized microporous structure of ePTFE membranes by controlling the particle size of PTFE fine powders for achieving high oil-water separation performances. *J. Memb. Sci.* **2021**, *629*, 119294. [CrossRef]
25. Yu, T.; Lu, S.; Xu, W.; Boukherroub, R. Preparation of superhydrophobic/superoleophilic copper coated titanium mesh with excellent ice-phobic and water-oil separation performance. *Appl. Surf. Sci.* **2019**, *476*, 353–362. [CrossRef]
26. Ko, T.-J.; Hwang, J.-H.; Davis, D.; Shawkat, M.S.; Han, S.S.; Rodriguez, K.L.; Oh, K.H.; Lee, W.H.; Jung, Y. Superhydrophobic MoS_2-based multifunctional sponge for recovery and detection of spilled oil. *Curr. Appl. Phys.* **2020**, *20*, 344–351. [CrossRef]
27. Pan, Y.; Zhu, T.; Xia, Q.; Yu, X.; Wang, Y. Constructing superhydrophobic ZIF-8 layer with bud-like surface morphology on PDMS composite membrane for highly efficient ethanol/water separation. *J. Environ. Chem. Eng.* **2021**, *9*, 104977. [CrossRef]
28. Kamelian, F.S.; Mohammadi, T.; Naeimpoor, F. Fast, facile and scalable fabrication of novel microporous silicalite-1/PDMS mixed matrix membranes for efficient ethanol separation by pervaporation. *Sep. Purif. Technol.* **2019**, *229*, 115820. [CrossRef]
29. Zhang, X.; Zhi, D.; Sun, L.; Zhao, Y.; Tiwari, M.K.; Carmalt, C.J.; Parkin, I.P.; Lu, Y. Super-durable, non-fluorinated superhydrophobic free-standing items. *J. Mater. Chem. A* **2018**, *6*, 357–362. [CrossRef]
30. Chatzigrigoriou, A.; Karapanagiotis, I.; Poulios, I. Superhydrophobic coatings based on siloxane resin and calcium hydroxide nanoparticles for marble protection. *Coatings* **2020**, *10*, 334. [CrossRef]
31. Li, G.; Mai, Z.; Shu, X.; Chen, D.; Liu, M.; Xu, W. Superhydrophobic/superoleophilic cotton fabrics treated with hybrid coatings for oil/water separation. *Adv. Compos. Hybrid Mater.* **2019**, *2*, 254–265. [CrossRef]
32. Saji, V.S. Electrophoretic-deposited superhydrophobic coatings. *Chem.—Asian J.* **2021**, *16*, 474–491. [CrossRef] [PubMed]
33. Gadermann, M.; Preston, T.; Troster, C.; Signorell, R. Characterization of palmitic and lauric acid aerosols from rapid expansion of supercritical CO_2 solutions. *Mol. Phys.* **2008**, *106*, 945–953. [CrossRef]
34. Jiesheng, L.; Yuanyuan, Y.; Xiang, H. Research on the preparation and properties of lauric acid/expanded perlite phase change materials. *Energy Build.* **2016**, *110*, 108–111. [CrossRef]
35. Nelson, P.N.; Taylor, R.A. Powder X-ray diffraction, infrared and 13C NMR spectroscopic studies of the homologous series of some solid-state zinc(II) and sodium(I) n-alkanoates. *Spectrochim. Acta Part A Mol. Biomol. Spectrosc.* **2015**, *138*, 800–806. [CrossRef]
36. Estruga, M.; Domingo, C.; Ayllón, J.A. Solution-processable ZnO nanoparticles obtained by low-temperature solventless synthesis. *J. Mater. Chem.* **2011**, *21*, 4408. [CrossRef]
37. Hermans, J.J.; Keune, K.; van Loon, A.; Iedema, P.D. An infrared spectroscopic study of the nature of zinc carboxylates in oil paintings. *J. Anal. At. Spectrom.* **2015**, *30*, 1600–1608. [CrossRef]

38. Liu, C.; Shih, K.; Gao, Y.; Li, F.; Wei, L. Dechlorinating transformation of propachlor through nucleophilic substitution by dithionite on the surface of alumina. *J. Soils Sediments* **2012**, *12*, 724–733. [CrossRef]
39. Serga, V.; Burve, R.; Krumina, A.; Romanova, M.; Kotomin, E.A.; Popov, A.I. Extraction—Pyrolytic method for TiO_2 polymorphs production. *Crystals* **2021**, *11*, 431. [CrossRef]
40. Sohrabi, S.; Keshavarz Moraveji, M.; Iranshahi, D. Morphological and structural insights into high aspect ratio lauric acid/TiO2 nanowires: A low-temperature synthesis. *Ceram. Int.* **2021**, *47*, 9424–9436. [CrossRef]
41. Xu, Q.; Hu, S.; Wang, W.; Wang, Y.; Ju, H.; Zhu, J. Temperature-induced structural evolution of Sm nanoparticles on Al_2O_3 thin film: An in-situ investigation using SRPES, XPS and STM. *Appl. Surf. Sci.* **2016**, 1–6. [CrossRef]
42. Men, S.; Jiang, X.; Xiang, X.; Sun, G.; Yan, Y.; Lyu, Z.; Jin, Y. Synthesis of cellulose long-chain esters in 1-butyl-3-methylimidazolium Acetate: Structure-property relations. *Polym. Sci. Ser. B* **2018**, *60*, 349–353. [CrossRef]
43. Xing, J.-H.; Xia, Z.-B.; Hu, J.-F.; Zhang, Y.-H.; Zhong, L. Growth and crystallization of titanium oxide films at different anodization modes. *J. Electrochem. Soc.* **2013**, *160*, C239–C246. [CrossRef]
44. Gautier, P.; Vallee, A.; Sinito, C.; Etcheberry, A.; Simon, N. Effect of growth temperature on the electrodeposition of zinc oxide layers on diamond surfaces. *Diam. Relat. Mater.* **2016**, *62*, 1–6. [CrossRef]
45. Liu, T.; Fei, X.; Hu, L.; Zhang, H.; Li, Y.; Duo, S. Effect of substrate surface pretreatment and annealing treatment on morphology, structure, optical and electrical properties of sputtered ZnO films. *Superlattices Microstruct.* **2015**, *83*, 604–617. [CrossRef]
46. Cassie, A.B.D.; Baxter, S. Wettability of porous surfaces. *Trans. Faraday Soc.* **1944**, *40*, 546. [CrossRef]
47. Milionis, A.; Loth, E.; Bayer, I.S. Recent advances in the mechanical durability of superhydrophobic materials. *Adv. Colloid Interface Sci.* **2016**, *229*, 57–79. [CrossRef]
48. Verho, T.; Bower, C.; Andrew, P.; Franssila, S.; Ikkala, O.; Ras, R.H.A. Mechanically durable superhydrophobic surfaces. *Adv. Mater.* **2011**, *23*, 673–678. [CrossRef] [PubMed]
49. Mortazavi, V.; Khonsari, M.M. On the degradation of superhydrophobic surfaces: A review. *Wear* **2017**, *372–373*, 145–157. [CrossRef]
50. Li, M.; Bian, C.; Yang, G.; Qiang, X. Facile fabrication of water-based and non- fluorinated superhydrophobic sponge for efficient separation of immiscible oil/water mixture and water-in-oil emulsion. *Chem. Eng. J.* **2019**, *368*, 350–358. [CrossRef]
51. Liu, W.; Cui, M.; Shen, Y.; Zhu, G.; Luo, L.; Li, M.; Li, J. Waste cigarette filter as nanofibrous membranes for on-demand immiscible oil/water mixtures and emulsions separation. *J. Colloid Interface Sci.* **2019**, *549*, 114–122. [CrossRef] [PubMed]
52. Thasma Subramanian, B.; Alla, J.P.; Essomba, J.S.; Nishter, N.F. Non-fluorinated superhydrophobic spray coatings for oil-water separation applications: An eco-friendly approach. *J. Clean. Prod.* **2020**, *256*, 120693. [CrossRef]
53. Rius-Ayra, O.; Llorca-Isern, N. A robust and anticorrosion non-fluorinated superhydrophobic aluminium surface for microplastic removal. *Sci. Total Environ.* **2021**, *760*, 144090. [CrossRef] [PubMed]
54. Rius-Ayra, O.; Biserova-Tahchieva, A.; LLorca-Isern, N. Surface-functionalised materials for microplastic removal. *Mar. Pollut. Bull.* **2021**, *167*, 112335. [CrossRef]